Materials Horizons

ROYAL SOCIETY OF CHEMISTRY

COMMUNICATION

View Article Online
View Journal | View Issue

Cite this: *Mater. Horiz.*, 2024, 11, 5419

Received 26th July 2024,
Accepted 9th August 2024

DOI: 10.1039/d4mh00979g

rsc.li/materials-horizons

Polyethylene glycol-decorated n-type conducting polymers with improved ion accessibility for high-performance organic electrochemical transistors†

Haoran Tang,‡[a] Yuanying Liang,‡[ab] Chi-Yuan Yang, *[c] Xi Luo,[a] Jiangkai Yu,[a] Kai Zhang, [a] Simone Fabiano *[c] and Fei Huang *[a]

High-performance n-type organic mixed ionic-electronic conductors (OMIECs) are essential for advancing complementary circuits based on organic electrochemical transistors (OECTs). Despite significant progress, current n-type OMIECs often exhibit lower transconductance and slower response times compared to their p-type counterparts, limiting the development of OECT-based complementary circuits. Optimizing the conjugated backbone and side chain structures of OMIECs is critical for enhancing both ion and electron transport efficiencies while maintaining a delicate balance between the two. In this study, hydrophilic polyethylene glycol (PEG) side chains were incorporated into the highly conductive n-type polymer poly(3,7-dihydrobenzo[1,2-*b*:4,5-*b*′]difuran-2,6-dione) (PBFDO) backbone to achieve this goal. The incorporation of PEG chains improved ion accessibility, and by adjusting the PEG content, the electronic and ionic transport properties were fine-tuned, ultimately enhancing the performance of OECTs and related p–n complementary circuits. The n-type OECTs based on PBFDO-PEG50wt% demonstrated exceptional transfer characteristics, including a transient response time (τ_{ON}) as low as 72 μs, a high geometry-normalized transconductance exceeding 400 S cm^{-1}, and an impressive μC^* value surpassing 720 F cm^{-1} V^{-1} s^{-1}. Notably, the use of PBFDO-PEG50wt% in a complementary inverter resulted in a voltage gain of 20 V/V, more than five times higher than that achieved with unmodified PBFDO (<4 V/V). These findings highlight the importance of balancing electron and ion transport characteristics in OMIECs to achieve high performance in OECTs and their associated circuits, and they validate PEG decoration as an effective approach.

New concepts

The development of low-voltage, biocompatible, flexible wearable electronic devices has introduced new challenges in materials science. Due to their intrinsic flexibility, biocompatibility, high volumetric capacitance, and excellent conductivity under electrochemical doping, organic mixed ionic-electronic conductors (OMIECs) are ideal material candidates for developing efficient organic electrochemical transistors (OECTs). Both p-type and n-type OMIECs are crucial for developing complementary circuits based on OECTs. However, the slower development of n-type OMIECs has limited progress in this area. Poly(3,7-dihydrobenzo [1,2-*b*:4,5-*b*′]difuran-2,6-dione) (PBFDO) stands out as one of the best performing n-type conducting polymers, boasting ultra-high conductivity exceeding 2000 S cm^{-1}. Despite this, its hydrophobic nature limits the development of high-speed OECTs. To overcome this, copolymerizing PBFDO with strongly hydrophilic building blocks can significantly enhance its hydrophilicity while preserving its charge carrier transport properties. By carefully designing these building blocks with hydrophilic side chains, the OECT's transient response and complementary inverter performance can be greatly improved. This advancement marks a substantial improvement over previous results and paves the way for future research in high-performance (bio-)electronic devices.

Introduction

Emerging π-conjugated systems capable of transporting both ionic and electronic charges, commonly known as organic mixed ionic-electronic conductors (OMIECs), have recently attracted considerable attention.[1–4] Specifically, with OMIECs

[a] *Institute of Polymer Optoelectronic Materials and Devices, State Key Laboratory of Luminescent Materials and Devices, Guangdong Basic Research Center of Excellence for Energy & Information Polymer Materials, South China University of Technology, Guangzhou 510640, China. E-mail: msfhuang@scut.edu.cn*
[b] *Guangdong Artificial Intelligence and Digital Economy Laboratory (Guangzhou), Guangzhou 510335, Guangdong, China*
[c] *Laboratory of Organic Electronics, Department of Science and Technology, Linköping University, SE-60174 Norrköping, Sweden. E-mail: chi-yuan.yang@liu.se, simone.fabiano@liu.se*

† Electronic supplementary information (ESI) available: Synthesis and characterization of the PEG unit and model compounds, calculation of surface energy and partial characterization of OECT devices. See DOI: https://doi.org/10.1039/d4mh00979g

‡ These authors contributed equally to this article.

as channel materials, organic electrochemical transistors (OECTs) have exerted their superior merits, including the ability to convert ionic fluxes into electronic signals, and the capacity to amplify and/or preserve signals through the construction of corresponding logic circuits.[5–9] The application of a gate voltage results in the injection of ions from the electrolyte into the OMIEC channels, and electrochemical doping within the entire channel, thus allowing for significant drain current modulations at low gate voltages (<1 V).[10,11]

The ability to convert variations in gate voltages into current modulations is referred to as transconductance, a key metric for assessing the performance of OECTs. Transconductance (g_m) is directly proportional to the carrier mobility (μ) and the capacitance per unit volume (C^*) of OMIECs. With the rapid advancement of OMIECs, the performance of OECTs has seen significant improvements, particularly in devices utilizing p-type OMIECs. These have demonstrated excellent performance, with normalized maximum transconductance ($g_{m,norm}$) surpassing 100 S cm^{-1} and figure-of-merit μC^* exceeding 500 F cm^{-1} V^{-1}.[12–14] However, the transconductance of n-type OMIECs has lagged behind, primarily due to limitations in n-doping ability and poor electron transport. These challenges have impeded the development of n-type OECTs and complementary circuits.[15–19]

Apart from transconductance, the mismatch in transient response between p-type and n-type OECTs presents another challenge in developing efficient complementary circuits. Currently, the response time of p-type OECTs is typically in the range of μs,[20,21] while n-type OECTs often surpass 10 ms.[22,23] According to the Bernard's model,[24] OECTs consist of both an ionic circuit that regulates ion movement within the gate-electrolyte-channel structure and an electronic circuit that governs the movement of charge carriers in the source–channel–drain structure. In practice, there is typically a trade-off between transconductance and response speed.[25] Enhanced electron transport and highly crystalline morphologies are often associated with high transconductance, while improved ion transport and disordered morphologies tend to favour a reduction in response times. Therefore, the electron transport and ion transport properties of n-type OMIECs need to be systematically tuned to achieve optimal performance in OECTs and complementary circuits.

In molecular structure design, backbones with strong electron-withdrawing capability are favoured for n-doping and electron transport.[26,27] Since the pioneering research utilizing naphthalene diimides (NDIs) as building blocks,[28] the transconductances of n-type OECTs have been effectively increased to over 150 S cm^{-1} through the development of backbone structures as well as doping state engineering.[22,23,29–34] In addition, side chain engineering is considered as an effective strategy to modulate ion transport. Polar side chains, such as ethylene glycol, can enhance ion penetration and improve device operation.[35,36] However, due to the insulating and disordered nature of the side chains themselves, introducing too many side chains may, in turn, affect the film stacking and degrade the electron transport properties of OMIEC materials.[37] To date, the development of n-type OMIECs possessing high transconductance and rapid response remains a significant yet formidable task.

In this work, motivated by the exceptional electron transport properties of the recently reported side-chain-free, highly conductive polymer poly(3,7-dihydrobenzo[1,2-*b*:4,5-*b*′]difuran-2,6-dione) (PBFDO),[38,39] we further incorporated varying amounts of polyethylene glycol (PEG) side chains into PBFDO to achieve a balance between electron and ion transport. The introduction of PEG significantly improves the hydrophilicity of PBFDO-based OMIECs, thereby improving its ion permeability, which accelerates the response speed of the resulting OECTs. As a result, we achieved record-high performance in n-type OECTs with swift response times. Moreover, by systematically adjusting the PEG content, we successfully balanced electrical performance and responsiveness, achieving a maximum transconductance of over 400 S cm^{-1}. In p–n complementary circuits, the PBFDO-PEG50wt% based devices exhibit superior signal amplification compared to those made with unmodified PBFDO. This work contributes to the advancement of n-type OMIECs and emphasizes the importance of optimizing the interplay between electron transport and ion accessibility in material design for constructing OECT complementary circuits.

Results and discussion

Fig. 1(a) shows the molecular structures and related performance of representative p-type and n-type OMIECs.[12,22,28,34,40] These materials are characterized by a combination of conjugated backbone and ethylene glycol side chains, which facilitate electron transport and ion accessibility, respectively. Despite these similarities, there remains a notable performance gap between n-type and p-type OMIECs. Of particular interest is the recently developed side-chain-free n-type conducting polymer PBFDO,[38,41] which has demonstrated superior electron transport properties and potential for facilitating the OECT performance comparable to its p-type counterparts.[42] However, the compact film stacking and hydrophobic nature of PBFDO hinder the migration of ions from the electrolyte into the channel film, leading to a slow OECT device response and constraining the feasibility of constructing p–n complementary circuits. To strike a balance between ion accessibility and electron transport ability, a copolymerization unit with PEG side chains (referred to as the PEG unit) has been developed. This unit can be copolymerized into the conjugated backbone of PBFDO through aldol condensation, resulting in the preparation of a series of polymers with varying proportions of PEG side chains, specifically denoted as PBFDO-PEG*x*wt% (x = 50, 100). The synthetic route and expected chemical structures of polymers are shown in Fig. 1(b). The unmodified polymer PBFDO was first synthesized from the 3,7-dihydrobenzo[1,2-*b*:4,5-*b*′]difuran-2,6-dione (H-BFDO) monomer in the presence of 2,3,5,6-tetramethylbenzoquinone (TMQ). Subsequently, different contents of copolymerization units with PEG side chains were introduced into the reaction system, enabling the incorporation of varying PEG content through

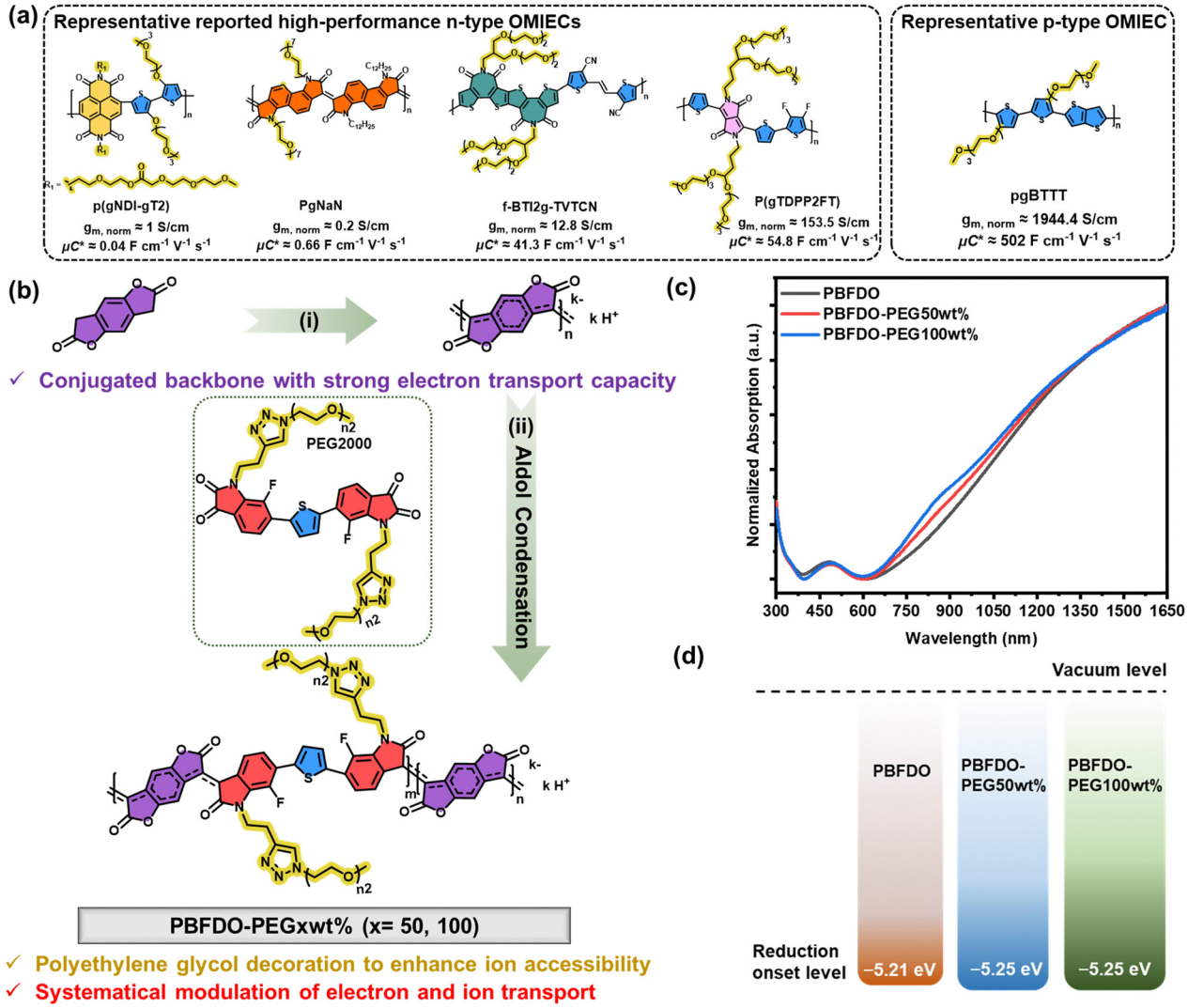

Fig. 1 (a) The molecular structures of representative p-and n-type OMIECs. (b) Schematic illustration of synthesis of PBFDO-PEG based OMIECs. (i) TMQ, DMSO, 85 °C, 6 h and (ii) injection of PEG units, 85 °C, 8 h. (c) Optical absorption spectra of the investigated OMIECs. (d) The energy level diagram of PBFDO-PEG based OMIECs.

aldol condensation with the reactive methylene group of either the H-BFDO or PBFDO end group. The detailed synthesis procedures and characterization techniques of the PEG copolymerization unit are shown in the ESI† (Fig. S1–S6). To verify the feasibility of aldol condensations,[43] control experiments including both a small molecule and a model polymer were conducted. The results shown in Fig. S7–S13 (ESI†) demonstrated the successful condensation of the carbonyl group in isatin derivatives with the methylene group of H-BFDO through simple heating in the polar solvent. The model copolymer of the PEG unit and the H-BFDO monomer exhibited a number-average molecular weight (M_n) of 381.8 kDa and a polydispersity index (PDI) of 1.55 (Fig. S13, ESI†). Nevertheless, as shown in Fig. S14 and S15 (ESI†), the M_n values of PEG side chain-decorated OMIECs PBFDO-PEG*x*wt% (x = 50, 100) were 10.7 and 9.9 kDa with corresponding PDIs of 11.05 and 13.45, respectively. The large weight-average molecular weight (M_w) and PDIs observed in PBFDO-PEG series polymers may be attributed to the concurrent occurrence of oxidative polymerization and aldol polycondensation after the addition of PEG units into the reaction mixture, each following distinct reaction mechanisms and kinetics. Additionally, it is important to acknowledge that the determination of molecular weight using gel permeation chromatography (GPC) should be approached cautiously, given the distinctive solubility characteristics of PBFDO series materials and the absence of suitable standards. The dynamics of rigid conjugated ladder polymers may deviate considerably from that of standard materials.[44] In order to assess the precise copolymerized content of PEG units, elemental analysis (EA) was conducted. As shown in Table S1 (ESI†), the nitrogen content of the polymer increased with increasing feeding weight ratio of PEG units as nitrogen is exclusively present in the PEG units. Consequently, considering the errors associated with EA, the copolymerization weight

ratios of the PEG units were estimated to be 54 wt% and 100 wt% for PBFDO-PEG*x*wt% (x = 50, 100), respectively, which were basically consistent with the feeding ratios.

UV-Visible absorption measurements were conducted to determine the effect of copolymerized PEG units on the absorption bands of the PBFDO-PEG series polymers. As shown in Fig. 1(c), pure PBFDO exhibits distinct absorption in the near-infrared (NIR) region, which can be attributed to the *in situ* n-doping effect during the reaction.[38,45] To further confirm the n-doped state of the PBFDO polymer, de-doping and re-doping experiments were conducted. As shown in Fig. S16 (ESI†), the immersion of the PBFDO film in a solution of the strong oxidant tris(4-bromophenyl)aminium hexachloroantimonate (magic blue) led to a disappearance of absorption in the near-infrared region, indicating the de-doping of the PBFDO. Subsequent immersion of the above de-doped film in a solution of tetramethylhydroquinone (TMQH) resulted in the reappearance of polaron absorption, verifying that TMQH, generated during oxidative polymerization, would facilitate *in situ* n-doping of the polymer. Additionally, increasing ratio of PEG copolymerization units resulted in an enhancement of absorption in the 750–900 nm range in PBFDO-PEG series polymers. To gain a deeper understanding of this absorption phenomenon, the absorption spectra of both the PEG unit and the model copolymer resulting from the aldol polycondensation of the H-BFDO monomer and the PEG unit were recorded. As shown in Fig. S17 (ESI†), the dominant absorption peak of the PEG unit was around 410 nm, while the model copolymer exhibited a strong characteristic absorption near 760 nm. Thus, the enhanced absorption at 750–900 nm observed in the PBFDO-PEG series polymers provided evidence that the PEG units were successfully incorporated into the conjugated backbone rather than simple co-blending.

Subsequently, cyclic voltammetry (CV) measurements were conducted in acetonitrile to determine the reduction onset levels using the ferrocene/ferrocenium (Fc/Fc^+) redox couple as an external reference. The deep reduction level contributes to the n-doping efficiency and n-doped state stabilization under the ambient environment, and generally, a level lower than −4.9 eV is required for thermodynamic stability of n-doping.[46,47] From the reduction onsets of CV curves (Fig. S18, ESI†), the reduction levels of PBFDO-PEG50wt% and PBFDO-PEG100wt% are both calculated to be −5.25 eV (Fig. 1(d)), which are low enough to ensure the ambient stability of the n-doping state. Notably, given that the as-prepared PBFDO series polymers are inherently in an n-doped state, CV measurement was conducted on the de-doped PBFDO film to ascertain its lowest unoccupied molecular orbital (LUMO) energy level. As shown in Fig. S19 (ESI†), the de-doped film underwent reduction at significantly high potentials, indicating that the neutral PBFDO possessed a deeper LUMO level, which explained its tendency to undergo *in situ* n-doping during the reaction.

Prior to device performance evaluation, the morphology and microstructures of these OMIECS were characterized. The surface morphology of PBFDO-PEG-based films was evaluated using an atomic force microscope (AFM). As shown in Fig. 2(a), all polymer films are smooth with a small root-mean-square roughness (R_q) varying from 1.37 to 2.10 nm, indicating that the incorporation of PEG side chains does not affect the roughness significantly. In order to quantitatively evaluate the effect of different contents of PEG on the surface properties of films, the contact angles of water and diiodomethane (DIM) droplets on the surfaces were measured and the surface energies (γ_S) were calculated with the equation reported previously.[48] A detailed calculation procedure is shown in the ESI† and Table S2. As shown in Fig. 2(b), the contact angles of water droplets on films decline from PBFDO (79.3°) to PBFDO-PEG50wt% (69.4°) and PBFDO-PEG100wt% (64.0°), corresponding to an increased γ_S from 40.91 to 44.11 and 48.53 mN m^{-1}, respectively. This enhancement promotes effective contact with the electrolyte aqueous solution and thus facilitates ion migration in OECT devices.

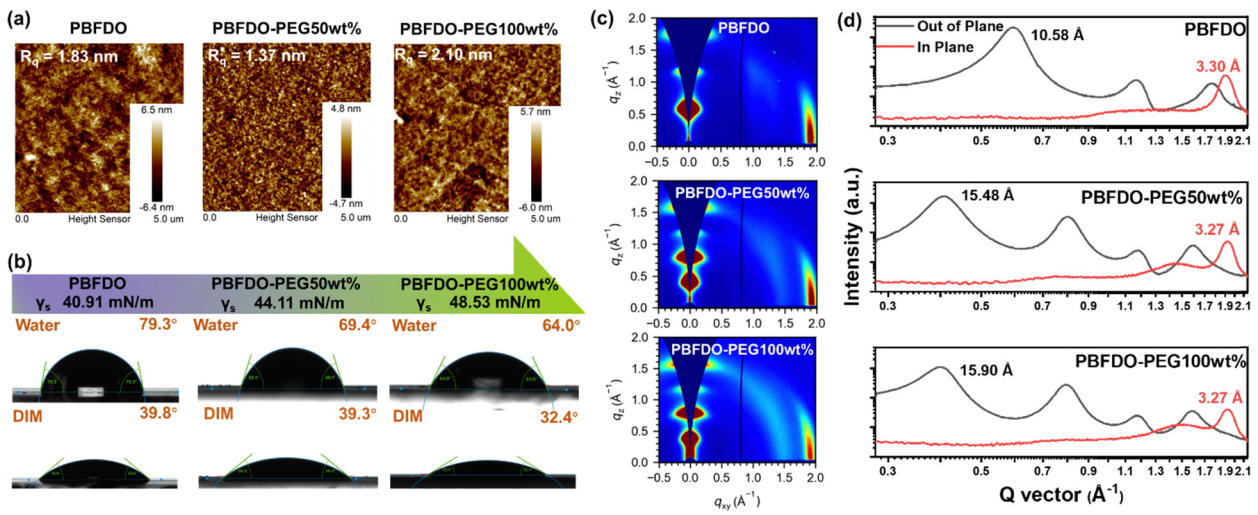

Fig. 2 (a) Atomic force microscopy height images of PBFDO-PEG films on glass substrates. (b) Contact angles and surface energies of PBFDO-PEG OMIECs. (c) and (d) 2D-GIWAXS images of PBFDO-PEG-based films and corresponding profiles along the in plane and out of plane directions.

To investigate the influence of PEG chains on the microstructure of polymer films, grazing incidence wide-angle X-ray scattering (GIWAXS) characterization techniques were performed (Fig. 2(c) and (d)). Pure PBFDO film primarily adopted an ordered edge-on packing structure on the substrate, which is favorable for planar transistor performance. The lamellar and π–π stacking distances of pure PBFDO were calculated to be 10.58 and 3.30 Å, respectively. Upon the introduction of a few PEG copolymerization units, the π–π stacking distance remained similar, while the original (100) diffraction peak at q_z = 0.594 $Å^{-1}$ disappeared. Instead, new diffraction peaks emerged, corresponding to the lamellar distances of 15.48 Å for PBFDO-PEG50wt% and 15.90 Å for PBFDO-PEG100wt%, respectively, which were about 5 Å larger than that of pure PBFDO, suggesting that PEG side chains mainly affect the lamella packing of PBFDO series polymers without interfering with π–π stacking. The expanded lamella distance is believed to facilitate rapid ion movement between polymer chains.

In situ electrochemistry spectral measurements were conducted to investigate the effect of introducing PEG side chains on the voltage-modulated electrochemical doping and de-doping process. These measurements, along with subsequent characterization techniques of OECT devices, were performed in $NaPF_6$ aqueous solution (0.1 M) to prevent potential charge transfer effects from halogen ions affecting film stability.[49,50] As illustrated in Fig. 3, de-doping the PBFDO-PEG films at 0.5 V resulted in a notable increase in absorption in the 500 nm and 700–900 nm regions, corresponding to the π–π* transition and intramolecular charge transfer (ICT) absorption, respectively. Furthermore, even after de-doping at 0.5 V, all three films still displayed strong absorption in the near-infrared region, suggesting the presence of polarons/bipolarons along the conjugated backbone and incomplete de-doping of the films at this voltage. Notably, the PEG-modified polymers (PBFDO-PEG50wt% and PBFDO-PEG100wt%) exhibit a significantly higher intrinsic absorption within the 700–900 nm range compared to the unmodified polymer (PBFDO) when subjected to the same de-doping potential, as illustrated in Fig. 3(a)–(c). This suggests that the incorporation of PEG side chains greatly enhances the capacity to regulate the doping state of OMIECs through voltage by facilitating the ion flow within the films. Additionally, as depicted in Fig. 3(d)–(f), a progressive reduction in the applied potential (from 0.5 V to −0.9 V) resulted in a noticeable decrease in the absorption intensity in the visible region. At a reduction potential lower than −0.2 V, the absorption associated with the π–π* transition and the ICT band were almost eradicated, indicating a highly n-doped state at these voltages.

The mixed electrical and ionic conduction performance of PBFDO-PEG OMIECs was then evaluated in OECT with the organic channel patterned on a glass substrate (Fig. 4). The devices were operated in 0.1 M $NaPF_6$ aqueous solution with a typical Ag/AgCl pellet as the gate electrode in ambient air. The application of a positive gate bias leads to a significant increase in the source–drain current (I_{ds}), indicating that devices operate in the accumulation mode. This enhancement can be attributed to the electrochemical doping process, wherein the conjugated chains are further doped by cations (Na^+) in the electrolyte promoted by voltage. The introduction of PEG side chains did not significantly impact the operation mode. However, slight decreases in the transfer characteristics,

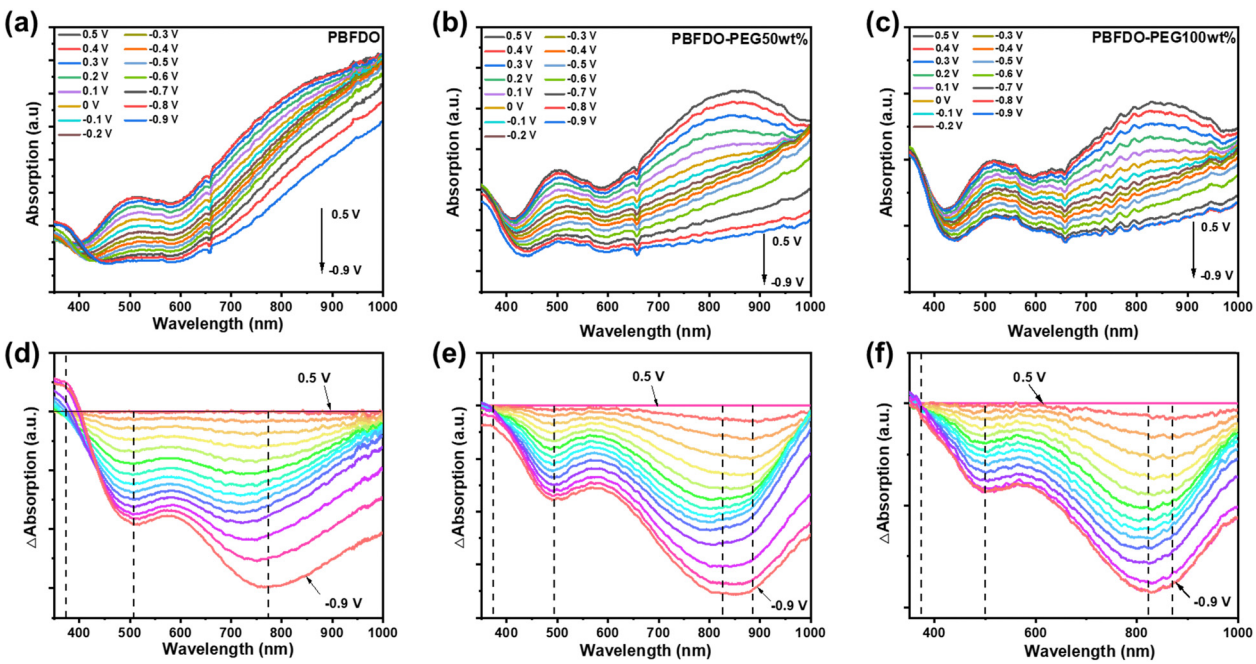

Fig. 3 Potential dependent UV-vis absorption spectra of the PBFDO-PEG/ITO electrode measured in 0.1 M $NaPF_6$ aqueous solution with Ag/AgCl as the reference electrode. (a)–(c) *In situ* UV-vis absorption spectra of PBFDO, PBFDO-PEG50wt% and PBFDO-PEG100wt%. (d)–(f) Corresponding differential absorption spectra at select voltages during CV scan.

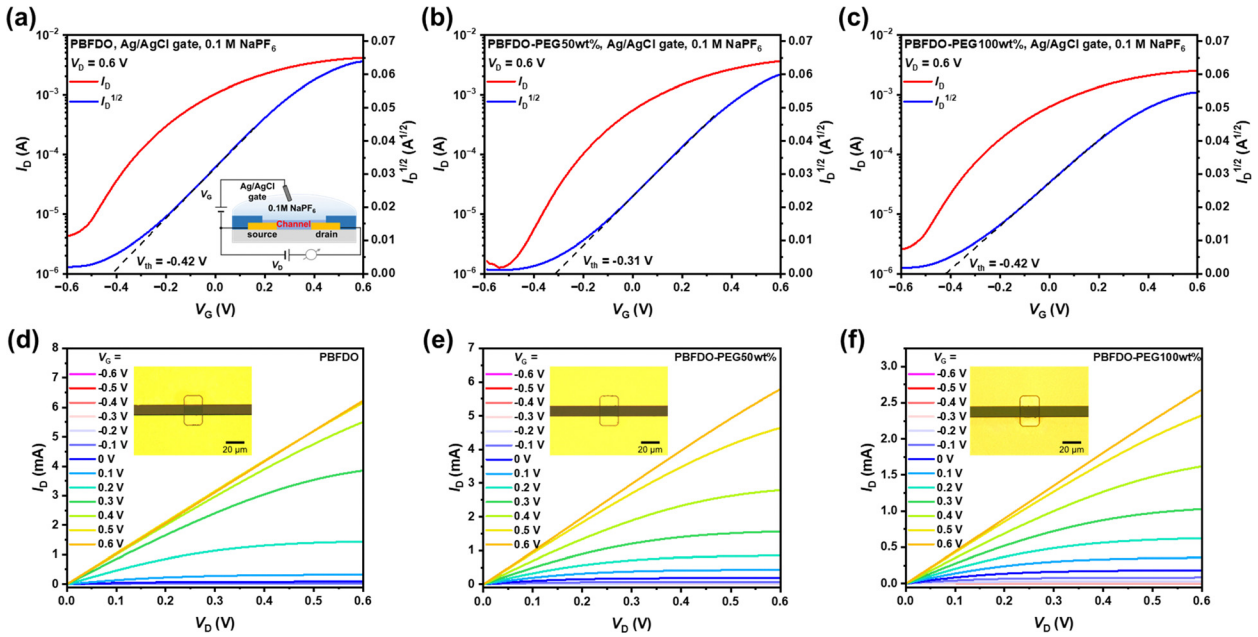

Fig. 4 Transfer (a)–(c) and output characteristics (d)–(f) of OECTs based on (a) and (d) PBFDO; (b) and (e) PBFDO-PEG50wt%; (c) and (f) PBFDO-PEG100wt%. The transfer characteristics were measured at V_{ds} = 0.6 V. The channel dimension used for this measurement is channel width/length = 20 μm/10 μm, while the thickness was around 70 nm. Inset: Illustration of the OECT structure (a) and optical microscopic photos of the corresponding OECT channels (d)–(f).

especially the "ON" drain–source current ($I_{ds,on}$) and maximum normalized transconductance, were observed. For the device based on PBFDO-PEG100wt%, these values decreased from approximately 4.1 mA and 438 S cm^{-1} to approximately 2.9 mA and 265 S cm^{-1}, respectively. These decreases may be attributed to the presence of insulating PEG chains and increased lamellar distance. The μC^* product at the saturation regime was then examined to elucidate the reduction in transconductance caused by introduction of PEG units. The OECTs based on unmodified PBFDO exhibited a remarkable μC^* value of around 796 F cm^{-1} V^{-1} s^{-1}, while slight decreases were observed with increasing PEG content. Specifically, a μC^* value of 724 and 583 F cm^{-1} V^{-1} s^{-1} is obtained for OECTs based on PBFDO-PEG50wt% and PBFDO-PEG100wt%, respectively. Remarkably, notwithstanding this decline, the performance of all devices persists at a comparable and even superior level when compared to the presently documented state-of-the-art n-type OECTs,[17,23,34,37,51,52] which could be attributed to the excellent electron transport capability of the PBFDO backbone and dominant edge-on packing of the PBFDO-PEG series polymers as shown earlier.

In addition to high transconductance, the operational speed of transistors is another critical factor for their practical applications, particularly in the construction of complementary circuits where synchronization of response times between p-type and n-type transistors is necessary. The incorporation of hydrophilic PEG units improves the wettability (Fig. 2) and promotes the transfer of ions between the electrolyte and the organic channel,[6,53] thereby potentially expediting the response of PBFDO-PEG based OECTs. The transient response times (τ) were determined by characterizing the I_{ds} variation of the applied pulse on the gate electrode, ranging from 0 V to 0.6 V, and extracted from an exponential fitting of the I_{ds} curves to the applied pulse. As shown in Fig. 5, the unmodified PBFDO-based OECTs exhibited a transient time τ of 138 μs. In contrast, PBFDO-PEG50wt% and PBFDO-PEG100wt%-based devices exhibited a notable decrease in transient time, with values of 71.6 μs and 22.2 μs, respectively. Generally, high transconductance comes at the expense of slow response.[54] To assess this trade-off in n-type OECTs, the ratio of the maximum transconductance to the transient response time (g_m/τ) was evaluated. The parameters of the PBFDO-PEG series OMIECs are summarized in Table 1 and a comparison with some state-of-the-art n-type OMIECs is shown in Fig. S20 (ESI†). In comparison to unmodified PBFDO ($g_m/\tau = 4.4 \times 10^4$ mS s^{-1}), the PBFDO-PEG-based OECT exhibits improved response (8.6×10^4 mS s^{-1} for PBFDO-PEG50wt% and 1.8×10^5 mS s^{-1} for PBFDO-PEG100wt%), significantly surpassing the most n-type OECTs by several orders of magnitude.[22,23,28,30,34]

The enhanced wettability of the PBFDO-PEG series OMIECs contributes to fast ion transport within the channel, producing a n-type OECT featuring both high transconductance and fast response, thereby enabling the construction of p–n complementary inverters. Here, p-type OMIEC P(g$_4$2T-TT) was utilized to fabricate the p-type accumulation-mode transistor for complementary inverters. The transfer and output characteristics of P(g$_4$2T-TT)-based p-type devices were measured in a 0.1 M NaCl aqueous solution with an Ag/AgCl pellet as a gate electrode (Fig. S21, ESI†). The device exhibits a transconductance of 62.4 S cm^{-1} and a low V_T of −0.11 V. The transient response

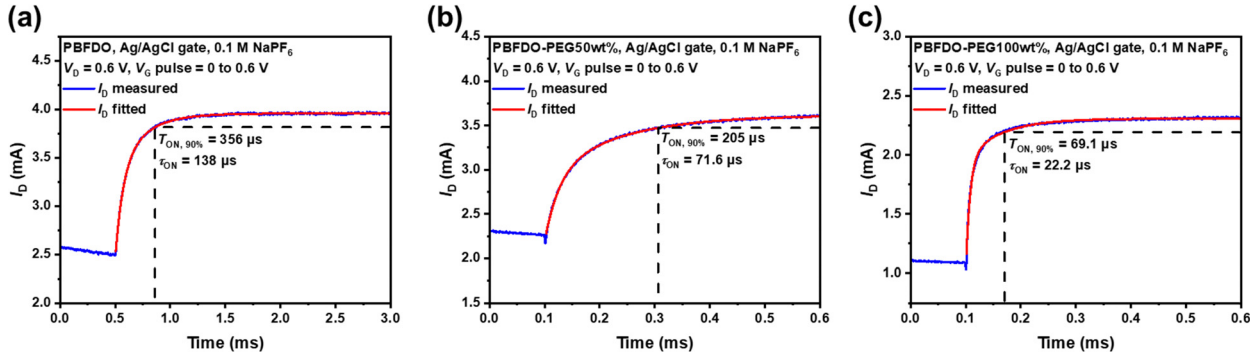

Fig. 5 Temporal response of the drain current (I_{ds}) of OECTs with different channel materials. (a) PBFDO; (b) PBFDO-PEG50wt%; (c) PBFDO-PEG100wt%. V_{gs} pulse amplitude = 0.6 V. V_G pulse stated from 0.5 ms (a) or 0.1 ms (b) and (c). $T_{ON,90}$ records the time required for the I_D to grow from the beginning of V_G pulse to 90% of the increase in I_D introduced by V_G pulse. τ_{ON} is the fitted time constant of the exponential decay curve.

Table 1 The device performance based on PBFDO and its PEG derivates

	$g_{m,norm}$ (S cm^{-1})	τ_{on} (µs)	g_m/τ (mS s^{-1})	V_T (V)	μC^{*a} (F V^{-1} cm^{-1} s^{-1})	$I_{d,on/off}$
PBFDO	438	138	4.4×10^4	−0.42	796	2×10^3
PBFDO-PEG50wt%	412	71.6	8.6×10^4	−0.31	724	2×10^3
PBFDO-PEG100wt%	265	22.2	1.8×10^5	−0.42	583	1×10^3

[a] μC^* product was extracted from the linear portion of $\sqrt{I_d}$ *versus* V_g curves according to the equation: $\sqrt{(I_d)} = (V_T - V_g) \times \sqrt{((wd/2l)\mu C^*)}$.

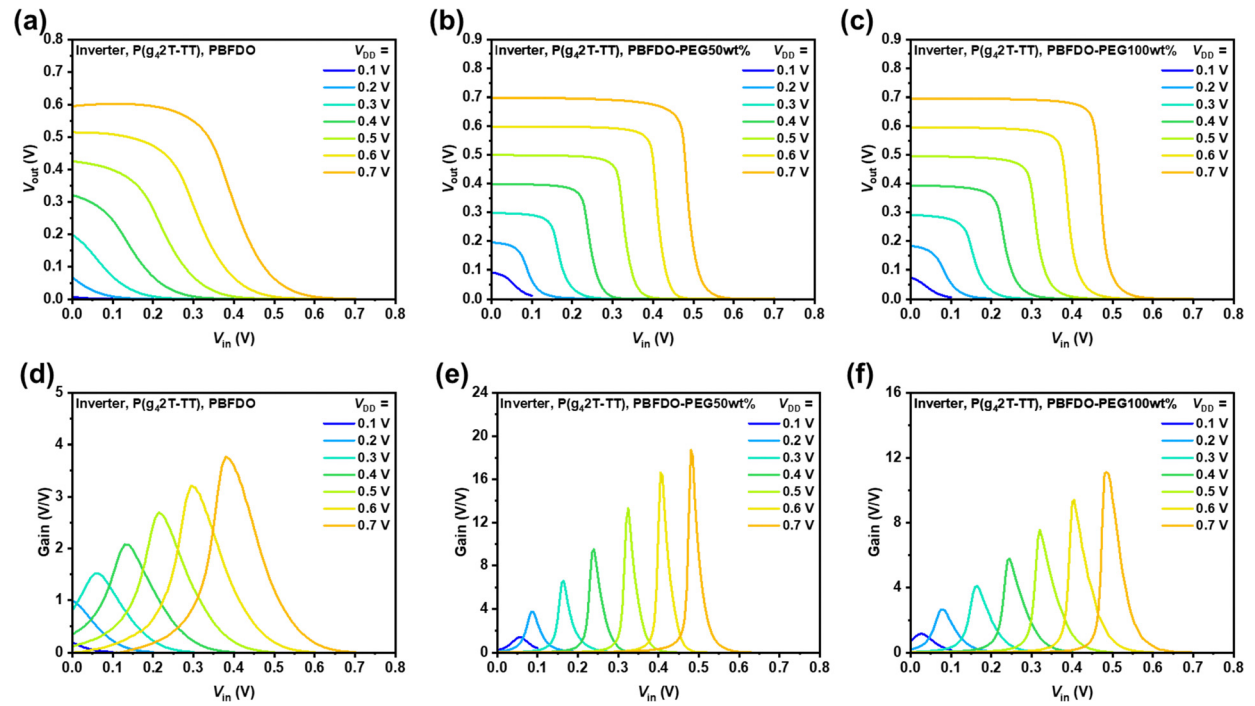

Fig. 6 OECTs-based complementary inverters. The voltage transfer characteristics and gain of inverters based on P(g$_4$2T-TT) with different n-type channel materials (a) and (d) PBFDO, (b) and (e) PBFDO-PEG50wt%, (c) and (f) PBFDO-PEG100wt%.

time of the P(g$_4$2T-TT)-based OECT was reported to be 74 µs, which could be well matched with PBFDO-PEG.[23] The inverting characteristics of P(g$_4$2T-TT)/PBFDO-based inverters are shown in Fig. 6. Remarkably, PBFDO-PEG50wt% based inverters exhibited voltage gains of 20 V/V, a value more than five times greater than that of unmodified PBFDO (<4 V/V) at the supply voltage (V_{DD}) = 0.7 V (Fig. 6(d) and (e)). In contrast, inverters based on PBFDO-PEG100wt% exhibited slightly lower voltage gains of approximately 12 V/V. These results indicate that appropriate PEG decoration was required to finely modulate ionic conduction of n-type OMIECs without substantially compromising the electronic conduction properties, which was anticipated

pushing forward the development of high-performance complementary circuits.

Conclusions

In summary, utilizing the high-performance n-type polymer PBFDO as a foundation, a group of conductive OMIECs bearing PEG side chains have been developed through a combination of oxidative polymerization and aldol polycondensation. This series of polymers, denoted as PBFDO-PEG*x*wt%, exhibits a deep-lying reduction level similar to that of PBFDO, facilitating efficient electron transport within OECT channels and promoting n-doping stability. Additionally, the decoration of PEG side chains enhances the ionic accessibility of OMIECs, leading to a significant acceleration in the response behavior of OECTs. By regulating the content of PEG copolymerization units, a favorable equilibrium between electron and ion transport in n-type OMIECs can be achieved. Consequently, PBFDO-PEG50wt%-based OECT devices exhibited a rapid response time τ_{ON} of 72 μs while maintaining good electron transport performance, achieving a high $g_{m,norm}$ of 412 S cm^{-1} and an exceptional μC^* value of 724 F cm^{-1} V^{-1} s^{-1}, which signify one of the most superior performance for n-type planar OECT devices. Notably, when further combined with p-type OMIECs to prepare complementary inverters, PBFDO-PEG50wt% based devices yield a significantly high voltage gain of near 20 V/V, surpassing that observed in the unmodified polymer. These findings highlight the significance of achieving a balance between electron and ion transport in n-type OMIECs and provide practical guidance for designing high-performance n-type OMIECs and their associated complementary circuits.

Experimental

Materials

6-Bromo-7-fluoro-2,3-dihydro-1*H*-indole-2,3-dione and 4-bromo-1-butyne were purchased from Shanghai Bide Pharmatech Ltd. 2,5-Bis(trimethylstannyl)thiophene was purchased from Suna-Tech Inc. The MPEG-N_3 (M.W. = 2000) was purchased from Shanghai Ponsure Biological Inc. Tris(4-bromophenyl)aminium hexachloroantimonate was purchased from Sigma Aldrich. Tetramethylhydroquinone was purchased from Shanghai Aladdin Biochemical Technology Co., Ltd. Anhydrous *N*,*N*-dimethylformamide (DMF) and other reagents and chemicals that were not specifically identified were purchased from Energy Chemical. The pure PBFDO was synthesized following a modified procedure.[38] In brief, the compounds H-BFDO (1 equiv.) and 2,3,5,6-tetramethylbenzo-1,4-quinone (TMQ, 1.65 equiv.) were introduced into the Schlenk flask. Subsequently, anhydrous dimethyl sulfoxide (DMSO) was added to solubilize the reactants. The concentration of H-BFDO in the final solution was 15 mg mL^{-1}. The reaction mixture was heated at 85 °C under argon protection for approximately 8 hours. Subsequently, dialysis against DMSO was performed using dialysis bags with a cut-off molecular weight of 10 kDa. The concentration used for device fabrication was determined to be 8–10 mg mL^{-1}.

Synthesis of PBFDO-PEG OMIECs

The compounds H-BFDO (1 equiv.) and TMQ (1.6 equiv.) were mixed in the Schlenk flask. Subsequently, anhydrous DMSO was added to solubilize the reactants. The concentration of the H-BFDO monomer in the final solution was 13 mg mL^{-1}. The reaction mixture underwent six cycles of evacuation under vacuum and argon refilling. Then, the mixture was heated to 85 °C and stirred for approximately 6 hours. Subsequently, the reaction mixture was cooled to room temperature. Various weight ratios of PEG units were then dissolved in DMSO and introduced into the reaction under argon protection. The mixture was then heated to 85 °C for approximately 8 hours to complete the subsequent aldol polycondensation. Following this, dialysis against DMSO was performed and the resulting concentration was determined to be 8–10 mg mL^{-1}.

Materials characterization techniques

Gel permeation chromatography (GPC) measurements were conducted using Agilent PL-GPC50 with DMSO as eluent and dextran as standards. Optical absorption spectra were recorded using SHIMADZU UV-3600i Plus. Elemental analysis was conducted on an Elemantar Vario EL cube with the CHNS mode. Atomic force microscope (AFM) characterization techniques were performed on Bruker Innova. 2D GIWAXS measurements were carried out at beamline 7.3.3 in the South China University of Technology with X-ray beam incident at a grazing angle of 0.20°. The contact angle measurements were performed on KRUSS DAS100S. Cyclic voltammetry (CV) characterizations were performed using CHI660E in a 0.1 M tetrabutylammonium hexafluorophosphate (*n*-Bu_4NPF_6) anhydrous acetonitrile solution electrolyte. Three electrode configuration was utilized with OMIECs thick films-coated ITO electrodes as the working electrode, a platinum wire as the counter electrode, and saturated calomel electrode as the reference electrode. The scan rate was 50 mV s^{-1}. The redox potential of ferrocene was measured as a standard control. *In situ* UV-vis spectroelectrochemistry measurements were carried out utilizing an Ocean Insight spectrophotometer (QE65PRO) and an Autolab (M204). The PBFDO-PEG films-coated ITO was chosen as the working electrode, complemented by an Ag/AgCl pellet as the reference electrode, same as that used for OECT measurements, and a platinum wire as the counter electrode. The spectro-electrochemistry measurements were conducted in a quartz cuvette filled with a 0.1 M $NaPF_6$ as the electrolyte. Stepwise decreased constant potential applied on the Ag/AgCl pellet were maintained for 3 min to ensure the sufficient electrochemical doping at each potential.

OECTs and complementary inverters

OECTs were fabricated according to previously reported methods, including metallization, passivation, and patterning of the

organic channel materials.[23] Prior to the preparation of organic film, the substrate underwent a 2-minute treatment in oxygen plasma to enhance surface wettability. Subsequently, PBFDO-PEG solutions were spin-coated onto the pretreated substrate at a spin speed of 2000 rpm to obtain even films. The resulting wet films were then transferred into a vacuum oven and dried at 45 °C overnight to remove the left solvent. The transfer characteristics were measured at V_{ds} = 0.6 V. The channel dimension used for this measurement is channel width/length = 20 μm/10 μm, while the thickness was around 70 nm. The P($g_4$2T-T)-based OECTs were fabricated using the same procedures. The thicknesses of films were measured using the Bruker Dektak XTL profilometer, yielding final measured thickness of approximately 70 nm for PBFDO-PEG series and 100 nm for the P($g_4$2T-TT) film. An Ag/AgCl pellet electrode was utilized as the gate electrode for all OECTs. The complementary inverters were established by connecting the n-type OECTs and the P($g_4$2T-TT)-based p-type OECTs with silver paint. Transfer, output, transient response characteristics of OECTs, and the voltage transfer characteristics of inverters were performed using a Keithley 4200A semiconductor analyzer equipped with a 4225-PMU ultra-fast *I–V* module and 4225-RPM Remote Amplifier/Switch modules. For PBFDO-PEG series polymers-based n-type OECT, all measurements were carried out in 0.1 M $NaPF_6$ aqueous solution during electrochemical doping process, while 0.1 M NaCl aqueous solution was chosen as electrolyte for the P($g_4$2T-TT)-based OECTs. τ_{ON} is fitted from exponential curves $I_D = I_{D,0} + A\cdot\exp[-(t - t_0)/\tau_{ON}]$ or $I_D = I_{D,0} + A_1\cdot\exp[-(t - t_0)/\tau_{ON,1}] + A_2\cdot\exp[-(t - t_0)/\tau_{ON,2}]$, and $\tau_{ON,average} = (A_1\cdot\tau_{ON,1} + A_2\cdot\tau_{ON,2})/(A_1 + A_2)$. $I_{D,0}$ is the drain current in V_G pulse off state, t_0 is the starting time of the V_G pulse on state, t is time, and A (and A_1, A_2) is the increasement of I_D.

Author contributions

H. Tang and Y. Liang contributed equally under the supervision of F. Huang. H. Tang conceived this work, synthesized, and characterized the materials. Y. Liang prepared OECT devices and measured *in situ* electrochemistry spectra. C.-Y. Yang characterized OECT devices and complementary circuits. X. Luo helped with material synthesis and characterization. J. Yu and K. Zhang helped with device measurements. H. Tang, Y. Liang, C.-Y. Yang, S. Fabiano and F. Huang wrote the manuscript. All authors contributed to discussion and manuscript preparation.

Data availability

The data supporting this article have been included as part of the ESI.†

Conflicts of interest

There are no conflicts to declare.

Acknowledgements

This work was financially supported by the Basic and Applied Basic Research Major Program of Guangdong Province (No. 2019B030302007), the National Natural Science Foundation of China (No. U21A6002), the National Youth Foundation of China (No. 52303227), the self-supporting project of Pa-zhou Lab (No. PZL2023ZZ0011), the Swedish Research Council (2020-03243, 2022-04053, and 2022-04553), the Knut and Alice Wallenberg Foundation (2021.0058, 2022.0034, and 2023.0464), and the Swedish Government Strategic Research Area in Materials Science on Functional Materials at Linköping University (Faculty Grant SFO-Mat-LiU 2009-00971). The authors wish to thank Assoc. Prof. Renee Kroon (Linköping University) for providing the p-type polymer P($g_4$2T-TT).

Notes and references

1 B. D. Paulsen, K. Tybrandt, E. Stavrinidou and J. Rivnay, *Nat. Mater.*, 2020, **19**, 13–26.
2 N. A. Kukhta, A. Marks and C. K. Luscombe, *Chem. Rev.*, 2022, **122**, 4325–4355.
3 A. Koklu, D. Ohayon, S. Wustoni, V. Druet, A. Saleh and S. Inal, *Chem. Rev.*, 2022, **122**, 4581–4635.
4 E. J. Fuller, S. T. Keene, A. Melianas, Z. Wang, S. Agarwal, Y. Li, Y. Tuchman, C. D. James, M. J. Marinella, J. J. Yang, A. Salleo and A. A. Talin, *Science*, 2019, **364**, 570–574.
5 J. Rivnay, S. Inal, A. Salleo, R. M. Owens, M. Berggren and G. G. Malliaras, *Nat. Rev. Mater.*, 2018, **3**, 17086.
6 E. Zeglio and O. Inganäs, *Adv. Mater.*, 2018, **30**, 1800941.
7 J. Chen, W. Huang, D. Zheng, Z. Xie, X. Zhuang, D. Zhao, Y. Chen, N. Su, H. Chen, R. M. Pankow, Z. Gao, J. Yu, X. Guo, Y. Cheng, J. Strzalka, X. Yu, T. J. Marks and A. Facchetti, *Nat. Mater.*, 2022, **21**, 564–571.
8 A. T. Lill, D. X. Cao, M. Schrock, J. Vollbrecht, J. Huang, T. Nguyen-Dang, V. V. Brus, B. Yurash, D. Leifert, G. C. Bazan and T.-Q. Nguyen, *Adv. Mater.*, 2020, **32**, 1908120.
9 S. Y. Jeong, J. W. Moon, S. Lee, Z. Wu, S. H. Park, J. H. Cho and H. Y. Woo, *Adv. Electron. Mater.*, 2023, **9**, 2300053.
10 C. M. Proctor, J. Rivnay and G. G. Malliaras, *J. Polym. Sci., Part B: Polym. Phys.*, 2016, **54**, 1433–1436.
11 D. Khodagholy, J. Rivnay, M. Sessolo, M. Gurfinkel, P. Leleux, L. H. Jimison, E. Stavrinidou, T. Herve, S. Sanaur, R. M. Owens and G. G. Malliaras, *Nat. Commun.*, 2013, **4**, 2133.
12 R. K. Hallani, B. D. Paulsen, A. J. Petty, II, R. Sheelamanthula, M. Moser, K. J. Thorley, W. Sohn, R. B. Rashid, A. Savva, S. Moro, J. P. Parker, O. Drury, M. Alsufyani, M. Neophytou, J. Kosco, S. Inal, G. Costantini, J. Rivnay and I. McCulloch, *J. Am. Chem. Soc.*, 2021, **143**, 11007–11018.
13 B. T. DiTullio, L. R. Savagian, O. Bardagot, M. De Keersmaecker, A. M. Österholm, N. Banerji and J. R. Reynolds, *J. Am. Chem. Soc.*, 2023, **145**, 122–134.
14 L. Lan, J. Chen, Y. Wang, P. Li, Y. Yu, G. Zhu, Z. Li, T. Lei, W. Yue and I. McCulloch, *Chem. Mater.*, 2022, **34**, 1666–1676.

15 P. Romele, P. Gkoupidenis, D. A. Koutsouras, K. Lieberth, Z. M. Kovács-Vajna, P. W. M. Blom and F. Torricelli, *Nat. Commun.*, 2020, **11**, 3743.
16 H. Sun, M. Vagin, S. Wang, X. Crispin, R. Forchheimer, M. Berggren and S. Fabiano, *Adv. Mater.*, 2018, **30**, 1704916.
17 J. Guo, L. Q. Flagg, D. K. Tran, S. E. Chen, R. Li, N. B. Kolhe, R. Giridharagopal, S. A. Jenekhe, L. J. Richter and D. S. Ginger, *J. Am. Chem. Soc.*, 2023, **145**, 1866–1876.
18 D. Ohayon, G. Nikiforidis, A. Savva, A. Giugni, S. Wustoni, T. Palanisamy, X. Chen, I. P. Maria, E. Di Fabrizio, P. M. F. J. Costa, I. McCulloch and S. Inal, *Nat. Mater.*, 2020, **19**, 456–463.
19 X. Wu, T. L. D. Tam, S. Chen, T. Salim, X. Zhao, Z. Zhou, M. Lin, J. Xu, Y.-L. Loo and W. L. Leong, *Adv. Mater.*, 2022, **34**, 2206118.
20 H. Jia, Z. Huang, P. Li, S. Zhang, Y. Wang, J.-Y. Wang, X. Gu and T. Lei, *J. Mater. Chem. C*, 2021, **9**, 4927–4934.
21 J. Rivnay, P. Leleux, M. Ferro, M. Sessolo, A. Williamson, D. A. Koutsouras, D. Khodagholy, M. Ramuz, X. Strakosas, R. M. Owens, C. Benar, J.-M. Badier, C. Bernard and G. G. Malliaras, *Sci. Adv.*, 2015, **1**, e1400251.
22 K. Feng, W. Shan, J. Wang, J.-W. Lee, W. Yang, W. Wu, Y. Wang, B. J. Kim, X. Guo and H. Guo, *Adv. Mater.*, 2022, **34**, 2201340.
23 H.-Y. Wu, C.-Y. Yang, Q. Li, N. B. Kolhe, X. Strakosas, M.-A. Stoeckel, Z. Wu, W. Jin, M. Savvakis, R. Kroon, D. Tu, H. Y. Woo, M. Berggren, S. A. Jenekhe and S. Fabiano, *Adv. Mater.*, 2022, **34**, 2106235.
24 D. A. Bernards and G. G. Malliaras, *Adv. Funct. Mater.*, 2007, **17**, 3538–3544.
25 J. Rivnay, P. Leleux, M. Ferro, M. Sessolo, A. Williamson, D. A. Koutsouras, D. Khodagholy, M. Ramuz, X. Strakosas, R. M. Owens, C. Benar, J.-M. Badier, C. Bernard and G. G. Malliaras, *Sci. Adv.*, 2015, **1**, e1400251.
26 R. Di Pietro, D. Fazzi, T. B. Kehoe and H. Sirringhaus, *J. Am. Chem. Soc.*, 2012, **134**, 14877–14889.
27 B. A. Jones, A. Facchetti, M. R. Wasielewski and T. J. Marks, *J. Am. Chem. Soc.*, 2007, **129**, 15259–15278.
28 A. Giovannitti, C. B. Nielsen, D.-T. Sbircea, S. Inal, M. Donahue, M. R. Niazi, D. A. Hanifi, A. Amassian, G. G. Malliaras, J. Rivnay and I. McCulloch, *Nat. Commun.*, 2016, **7**, 13066.
29 S. Cong, J. Chen, L. Wang, L. Lan, Y. Wang, H. Dai, H. Liao, Y. Zhou, Y. Yu, J. Duan, Z. Li, I. McCulloch and W. Yue, *Adv. Funct. Mater.*, 2022, **32**, 2201821.
30 K. Feng, W. Shan, S. Ma, Z. Wu, J. Chen, H. Guo, B. Liu, J. Wang, B. Li, H. Y. Woo, S. Fabiano, W. Huang and X. Guo, *Angew. Chem., Int. Ed.*, 2021, **60**, 24198–24205.
31 J. Shi, P. Li, X.-Y. Deng, J. Xu, Z. Huang, Y. Lei, Y. Wang, J.-Y. Wang, X. Gu and T. Lei, *Chem. Mater.*, 2022, **34**, 864–872.
32 Z. S. Parr, J. Borges-González, R. B. Rashid, K. J. Thorley, D. Meli, B. D. Paulsen, J. Strzalka, J. Rivnay and C. B. Nielsen, *Adv. Mater.*, 2022, **34**, 2107829.
33 Y. Wang, E. Zeglio, L. Wang, S. Cong, G. Zhu, H. Liao, J. Duan, Y. Zhou, Z. Li, D. Mawad, A. Herland, W. Yue and I. McCulloch, *Adv. Funct. Mater.*, 2022, **32**, 2111439.
34 P. Li, J. Shi, Y. Lei, Z. Huang and T. Lei, *Nat. Commun.*, 2022, **13**, 5970.
35 A. Giovannitti, D.-T. Sbircea, S. Inal, C. B. Nielsen, E. Bandiello, D. A. Hanifi, M. Sessolo, G. G. Malliaras, I. McCulloch and J. Rivnay, *Proc. Natl. Acad. Sci. U. S. A.*, 2016, **113**, 12017–12022.
36 D. Jeong, M. J. Kim, S. Lee, J.-W. Lee, Y. Kim, H. J. Kim, J. H. Cho and B. J. Kim, *Sci. China: Chem.*, 2022, **65**, 973–978.
37 J. Duan, G. Zhu, L. Wang, J. Chen, S. Cong, X. Zhu, Y. Zhou, Z. Li, I. McCulloch and W. Yue, *Adv. Funct. Mater.*, 2022, **32**, 2203937.
38 H. Tang, Y. Liang, C. Liu, Z. Hu, Y. Deng, H. Guo, Z. Yu, A. Song, H. Zhao, D. Zhao, Y. Zhang, X. Guo, J. Pei, Y. Ma, Y. Cao and F. Huang, *Nature*, 2022, **611**, 271–277.
39 H. Tang, H. Cai, H. Zhao, Z. Liu, R. Tan and F. Huang, *CCS Chem.*, 2023, **5**, 2534–2544.
40 X. Chen, A. Marks, B. D. Paulsen, R. Wu, R. B. Rashid, H. Chen, M. Alsufyani, J. Rivnay and I. McCulloch, *Angew. Chem., Int. Ed.*, 2021, **60**, 9368–9373.
41 Z. Ke, A. Abtahi, J. Hwang, K. Chen, J. Chaudhary, I. Song, K. Perera, L. You, K. N. Baustert, K. R. Graham and J. Mei, *J. Am. Chem. Soc.*, 2023, **145**, 3706–3715.
42 Y. Liang, C. Che, H. Tang, K. Zhang, L. Lan, C. Zhou, Y. Ma and F. Huang, *ACS Appl. Mater. Interfaces*, 2024, **16**, 19977–19986.
43 Q. Che, W. Zhang, X. Wei, Y. Zhou, H. Luo, J. Wei, L. Wang and G. Yu, *CCS Chem.*, 2023, **5**, 2603–2616.
44 M. Odziomek, P. Giusto, J. Kossmann, N. V. Tarakina, J. Heske, S. M. Rivadeneira, W. Keil, C. Schmidt, S. Mazzanti, O. Savateev, L. Perdigón-Toro, D. Neher, T. D. Kühne, M. Antonietti and N. López-Salas, *Adv. Mater.*, 2022, **34**, 2206405.
45 Z. Ke, J. Chaudhary, L. Q. Flagg, K. N. Baustert, A. O. Yusuf, G. Liu, L. You, K. R. Graham, D. M. DeLongchamp and J. Mei, *Adv. Funct. Mater.*, 2024, 2400255.
46 D. M. de Leeuw, M. M. J. Simenon, A. R. Brown and R. E. F. Einerhand, *Synth. Met.*, 1997, **87**, 53–59.
47 D. Yuan, W. Liu and X. Zhu, *Chem. Soc. Rev.*, 2023, **52**, 3842–3872.
48 D. K. Owens and R. C. Wendt, *J. Appl. Polym. Sci.*, 1969, **13**, 1741–1747.
49 X. Zhao, D. Madan, Y. Cheng, J. Zhou, H. Li, S. M. Thon, A. E. Bragg, M. E. DeCoster, P. E. Hopkins and H. E. Katz, *Adv. Mater.*, 2017, **29**, 1606928.
50 Z. Chen, Z. Hu, Z. Wu, X. Liu, Y. Jin, M. Xiao, F. Huang and Y. Cao, *J. Mater. Chem. A*, 2017, **5**, 19447–19455.
51 A. Marks, X. Chen, R. Wu, R. B. Rashid, W. Jin, B. D. Paulsen, M. Moser, X. Ji, S. Griggs, D. Meli, X. Wu, H. Bristow, J. Strzalka, N. Gasparini, G. Costantini, S. Fabiano, J. Rivnay and I. McCulloch, *J. Am. Chem. Soc.*, 2022, **144**, 4642–4656.
52 K.-K. Liu, P. Li, Y. Lei, Z. Zhang, X. Pan, S. K. So and T. Lei, *Adv. Funct. Mater.*, 2023, **33**, 2300049.
53 P. Das, R. Elizalde-Segovia, B. Zayat, C. Z. Salamat, G. Pace, K. Zhai, R. C. Vincent, B. S. Dunn, R. A. Segalman, S. H. Tolbert, S. R. Narayan and B. C. Thompson, *Chem. Mater.*, 2022, **34**, 2672–2686.
54 P. R. Paudel, M. Skowrons, D. Dahal, R. K. Radha Krishnan and B. Lüssem, *Adv. Theory Simul.*, 2022, **5**, 2100563.

